Campylobacter jejuni Antimicrobial Resistance Profiles and Mechanisms Determined Using a Raman Spectroscopy-Based Metabolomic Approach

Luyao Ma,[a] Lei Chen,[a,b] Keng C. Chou,[b] Xiaonan Lu[a,c]

[a]Food, Nutrition and Health Program, Faculty of Land and Food Systems, The University of British Columbia, Vancouver, British Columbia, Canada
[b]Department of Chemistry, Faculty of Science, The University of British Columbia, Vancouver, British Columbia, Canada
[c]Department of Food Science and Agricultural Chemistry, Faculty of Agricultural and Environmental Sciences, McGill University, Sainte-Anne-de-Bellevue, Quebec, Canada

ABSTRACT Rapid identification of antimicrobial resistance (AMR) profiles and mechanisms is critical for clinical management and drug development. However, the current AMR detection approaches take up to 48 h to obtain a result. Here, we demonstrate a Raman spectroscopy-based metabolomic approach to rapidly determine the AMR profile of *Campylobacter jejuni*, a major cause of foodborne gastroenteritis worldwide. *C. jejuni* isolates with susceptible and resistant traits to ampicillin and tetracycline were subjected to different antibiotic concentrations for 5 h, followed by Raman spectral collection and chemometric analysis (i.e., second-derivative transformation analysis, hierarchical clustering analysis [HCA], and principal-component analysis [PCA]). The MICs obtained by Raman-2nd derivative transformation agreed with the reference agar dilution method for all isolates. The AMR profile of *C. jejuni* was accurately classified by Raman-HCA after treating bacteria with antibiotics at clinical susceptible and resistant breakpoints. According to PCA loading plots, susceptible and resistant strains showed different Raman metabolomic patterns for antibiotics. Ampicillin-resistant isolates had distinctive Raman signatures of peptidoglycan, which is related to cell wall synthesis. The ratio of saturated to unsaturated fatty acids in the lipid membrane layer of ampicillin-resistant isolates was higher than in susceptible ones, indicating more rigid envelope structure under ampicillin treatment. In comparison, tetracycline-resistant isolates exhibited prominent Raman spectral features associated with proteins and nucleic acids, demonstrating more active protein synthesis than susceptible strains with the presence of tetracycline. Taken together, Raman spectroscopy is a powerful metabolic fingerprinting technique for simultaneously revealing the AMR profiles and mechanisms of foodborne pathogens.

IMPORTANCE Metabolism plays the central role in bacteria to mediate the early response against antibiotics and demonstrate antimicrobial resistance (AMR). Understanding the whole-cell metabolite profiles gives rise to a more complete AMR mechanism insight. In this study, we have applied Raman spectroscopy and chemometrics to achieve a rapid, accurate, and easy-to-operate investigation of bacterial AMR profiles and mechanisms. Raman spectroscopy reduced the analysis time by an order of magnitude to obtain the same results achieved through traditional culture-based antimicrobial susceptibility approaches. It offers great benefits as a high-throughput screening method in food chain surveillance and clinical diagnostics. Meanwhile, the AMR mechanisms toward two representative antibiotic classes, namely, ampicillin and tetracycline, were revealed by Raman spectroscopy at the metabolome level. This approach is based on bacterial phenotypic responses to antibiotics, providing information complementary to that obtained by conventional

genetic methods such as genome sequencing. The knowledge obtained from Raman metabolomic data can be used in drug discovery and pathogen intervention.

KEYWORDS antimicrobial resistance, Raman spectroscopy, metabolomics, chemometric analysis, food safety, *Campylobacter jejuni*

Campylobacter jejuni is the most commonly reported bacterial pathogen for human zoonosis and causes a spectrum of diseases, from gastroenteritis to postinfectious complications such as Guillain-Barré syndrome (1–4). Although most *Campylobacter* infections are self-limiting, antibiotic therapies are required for immunocompromised patients and those with extraintestinal infections (e.g., bacteremia and meningitis). However, antimicrobial resistance (AMR) of *Campylobacter* has recently reached alarming levels and led to the failure and extension of clinical treatments (5, 6). For instance, approximately half of the clinical *C. jejuni* isolates were determined to be resistant to tetracycline and ampicillin, commonly used in empirical prescriptions for foodborne pathogen infections (7, 8).

To address the rising threat of AMR, several approaches have been attempted, such as improving diagnostics to guide antibiotic usage, establishing surveillance systems from the One Health perspective that involves the human, environment, and agri-food sectors, and developing new antimicrobials (9–11). One of the key issues for identifying *Campylobacter* AMR profiles is that the conventional culture-based antimicrobial susceptibility testing (AST) is time-consuming (~48 h) and labor-intensive (7). The gold standard method is not efficient for urgent disease diagnostics and national surveillance systems. Furthermore, understanding AMR mechanisms provides clues to develop novel antimicrobial drugs, especially AMR breakers (e.g., β-lactamase inhibitors to combat ampicillin-resistant bacteria) (12, 13). Current AMR mechanism investigations utilize gene cloning and genome sequence analyses to identify AMR determinants, requiring tedious experimental design and high-cost facilities (14–16). For instance, whole-genome sequencing was recently applied to identify AMR genes and predict the AMR of *C. jejuni* with a high degree of accuracy (up to 99%) (17, 18). However, the high cost and limited speed of inferring AMR from sequence data remain the major challenges to the widespread adoption of whole-genome sequencing (WGS)-based AST in the clinical settings (19). Therefore, a rapid and easy-to-use approach is required to improve the efficiency of diagnostics and mechanism discovery.

Raman spectroscopy has emerged as a nondestructive tool for cellular metabolomic profiling, with a spectrum acquisition time of a few seconds (20–23). A Raman spectrum describes vibrational signatures of molecules in bacteria, thereby deciphering the complete molecular composition of the entire cell. For example, Raman spectroscopy was recently used to monitor bacterial metabolite patterns upon antimicrobial treatments, revealing the antimicrobial susceptibility or antimicrobial modes of action (24–26). The biochemical features of *Campylobacter* have been revealed by Raman spectroscopy after exposing the bacteria to a diverse panel of antimicrobials, including antibiotics (27), garlic-derived organosulfur compounds (28), metal oxide nanoparticles (e.g., TiO_2, Al_2O_3, and ZnO) (29, 30), and essential oils (31). However, to our knowledge, no studies have utilized Raman spectroscopy to investigate AMR mechanisms in *Campylobacter*.

Here, we developed a novel antimicrobial susceptibility test (AST) for *C. jejuni* that not only determines the bacterial AMR profile but also identifies potential AMR-associated metabolic fingerprinting. Antimicrobial-susceptible and -resistant *C. jejuni* isolates were treated with two representative antibiotics with distinct modes of action (i.e., ampicillin and tetracycline). Bacterial phenotypic responses to antibiotics were investigated by a Raman-based metabolomic approach. Chemometric analyses were applied to extract bacterial biochemical information from Raman spectra to determine the MICs for tested strains and decipher the corresponding AMR metabolites.

RESULTS AND DISCUSSION

Determination of MICs by Raman spectroscopy-chemometric analysis. We investigated the feasibility of using Raman spectroscopy to determine the MICs of

different drug classes in *C. jejuni*. Ampicillin and tetracycline were selected as the representative antibiotics because of the high occurrence of resistance to these drugs (~50%) in *C. jejuni* strains isolated from both clinical and agri-food settings (7). Both antibiotics were routinely tested on *Campylobacter* isolates in national AMR surveillance systems, such as the Canadian Integrated Program for Antimicrobial Resistance Surveillance (CIPARS) (32). For each drug, both antibiotic-susceptible and antibiotic-resistant strains, namely, F38011 (ampicillin- and tetracycline-susceptible strain), 1463 (ampicillin-resistant strain), and 1143 (tetracycline-susceptible strain), were included in the Raman-based MIC test. To determine their MIC values, these bacteria were exposed to a range of antibiotic concentrations for 5 h, followed by Raman spectrum acquisition for 1 min. It is known that *C. jejuni* cells experience distinctive damage levels and stress responses at different antibiotic concentrations. Therefore, an alteration of Raman spectral features could be expected when the antimicrobial concentration increases from 0 mg/liter to a value above the MICs.

Figure 1 shows the Raman spectra of *C. jejuni* exposed to various concentrations of ampicillin. The developed method provided reproducible spectra as a narrow gray region, indicating that the low standard deviations were around the mean spectra of each test group (Fig. 1a and c). We observed a decrease in peak intensity at 723 cm^{-1} (adenine) and 778 cm^{-1} (uracil) when ampicillin concentrations increased (Fig. 1a and c) (33, 34). Compared to the positive control, the ampicillin-susceptible strain F38011 displayed significant peak reductions ($P < 0.05$) at 723 and 778 cm^{-1} when the ampicillin concentration was above 2 mg/liter, while the ampicillin-resistant strain 1463 showed significantly reduced peaks ($P < 0.05$) at 256 mg/liter (see Fig. S1 in the supplemental material). Less intensive DNA/RNA base-related peaks indicated the inhibition of bacterial growth at certain ampicillin levels. Similar trends were reported in previous studies on other bacteria, such as *Escherichia coli* and *Lactobacillus lactis* (35, 36). Other than these two Raman peaks, spectra appeared to be very similar in the remaining regions (Fig. 1a and c).

To better illustrate the variations between treatment groups, we applied PCA to the entire Raman spectral region (400 to 1,800 cm^{-1}). PCA reduces the dimensions of multivariate data sets into a small batch of uncorrelated variables, called principal components (PCs), while maintaining most of the variations in the data set. By using a few PCs, each sample is represented by relatively fewer variables (i.e., PCs) instead of thousands of original variables (i.e., Raman shifts). As a result, samples can be plotted by using the first two or three PCs that represent the most variances, making it possible to visually assess the differences among samples and determine if samples can be grouped (37). As an unsupervised classification method, PCA explores spectral variance patterns without referring to prior knowledge about whether the samples belong to different groups or have phenotypic differences (37), leading to a less biased result.

In the conventional culture-based AST, MIC is defined as the lowest antibiotic concentration that causes a visible bacterial population reduction. Phenotypic variance is expected to exist between the positive-control group (i.e., without antibiotics) and the MIC-treated group, whereas sub-MIC groups are indistinguishable from the nontreated group. Similarly, we hypothesized that the MIC determined by the Raman-PCA method should be the lowest antibiotic concentration that forms a cluster separated from the positive-control group in the PCA score plot (Fig. 1 and 2). To identify the clusters, the color shade of each treatment group was drawn based on the mean ± 2 standard deviations in all three PCs, representing a 95% confidence limit. Two clusters not overlapping indicated that the two clusters were significantly different ($P < 0.05$). Figure 1b and d demonstrate the PCA score plots for the ampicillin test. Each scattered data point was labeled with the corresponding antibiotic concentration. For ampicillin-susceptible strain F38011, a clear cluster separation was obtained between untreated cells and cells treated with 1 to 8 mg/liter ampicillin (Fig. 1b). The overlap between the control group and the group treated with a lower concentration of ampicillin (i.e., 0.5 mg/liter) suggested that there are negligible differences between their Raman spectra.
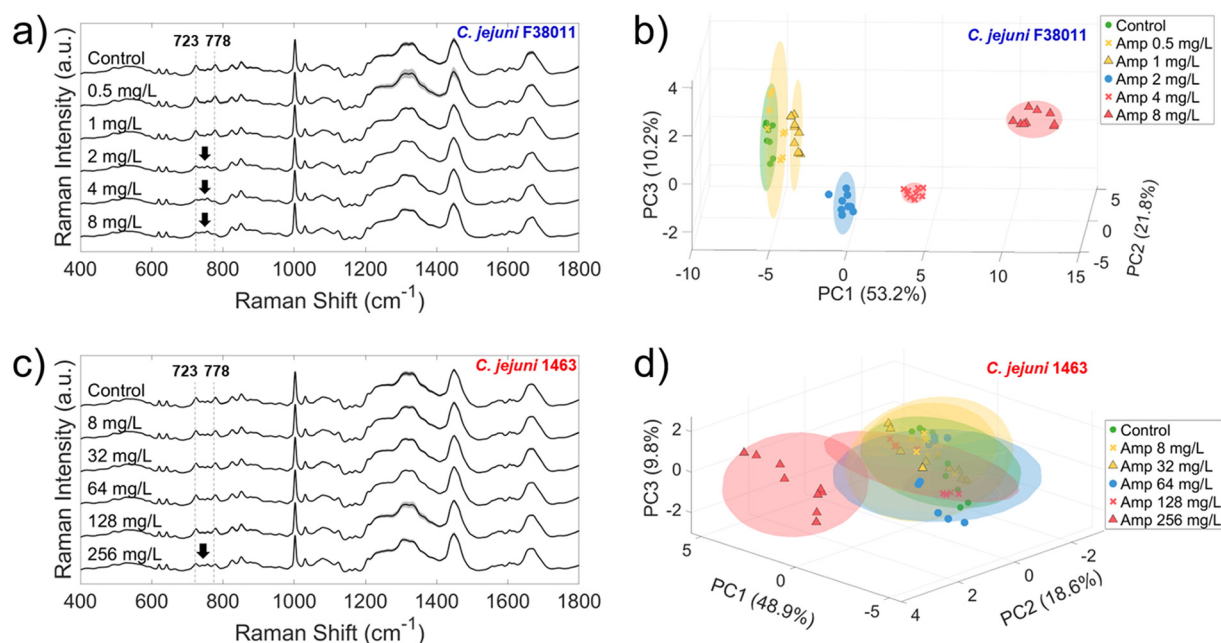
FIG 1 Determination of ampicillin MICs for *C. jejuni* using Raman spectroscopy-PCA. (a and b) Averaged Raman spectra (a) and PCA score plot (b) associated with a susceptible isolate, *C. jejuni* F38011, after treatments with ampicillin concentrations of 0, 0.5, 1, 2, 4, and 8 mg/liter. a.u., arbitrary units. (c and d) Averaged Raman spectra (c) and PCA (d) for a resistant isolate, *C. jejuni* 1463, after treatments with ampicillin concentrations of 0, 8, 32, 64, 128, and 256 mg/liter. Arrows in panels a and c indicate the significant changes in Raman spectral patterns. (b and d) Colored shades in PCA score plots were drawn as visual aids to illustrate the clusters of each group. It was calculated as the mean ± 2 standard deviations, representing a confidence limit of 95%. The MIC in the Raman-PCA method is defined as the lowest antibiotic concentration that induces Raman spectral changes compared to the positive-control group (i.e., green cluster). In plots shown in panels b and d, the MICs determined by Raman-PCA were 1 mg/liter and 256 mg/liter, respectively.

Therefore, the MIC of ampicillin for F38011 was determined to be 1 mg/liter based on the Raman-PCA method. For the ampicillin-resistant strain 1463, the MIC of ampicillin was identified to be 256 mg/liter, as this treatment group was segregated from other groups with concentrations lower than 128 mg/liter (Fig. 1d). To validate the accuracy of the Raman-PCA approach, the MICs were compared to those determined by the standard agar dilution method (7). If the MICs obtained by the reference and the newly developed methods are within a 2-fold dilution range, essential agreement between the two methods is regarded to have been achieved (38). The Raman-PCA reported a MIC comparable to that of the agar dilution method for the ampicillin-susceptible strain but a 4-fold higher MIC for the resistant strain (Table 1). However, both methods resulted in the same AMR profile category (i.e., resistant) when comparing the MICs to CLSI breakpoints (Table 1).

With the tetracycline MIC test, no apparent difference could be identified from the averaged Raman spectra (Fig. S2); therefore, we applied the Raman-PCA method to visually assess the MICs. The PCA score plots (Fig. 2) illustrated that tetracycline MICs were 0.06 mg/liter and 64 mg/liter for the susceptible strain (F38011) and the resistant strain (1143), respectively. For the susceptible strain, the MICs of tetracycline determined by Raman-PCA were consistent with those obtained by the reference method within a 2-fold dilution range (Table 1), reaching essential agreement with the reference method (38). Similar to the results for ampicillin, the Raman-PCA method reported a 4-fold higher MIC for tetracycline-resistant strains than the agar dilution method (Table 1).

Regardless of antibiotic class, Raman-PCA predicted a 4 times higher MIC value than the standard agar dilution method for resistant strains. The discrepancy of MICs was not solely caused by a shorter antibiotic treatment time for Raman-PCA (i.e., 5 h versus 48 h), since the amount of viable tetracycline-resistant bacteria was already significantly reduced ($P < 0.05$) after a 5-h incubation at the reference MIC value (Fig. S3). Noticeably, both resistant strains had MICs around their resistant breakpoints, namely,
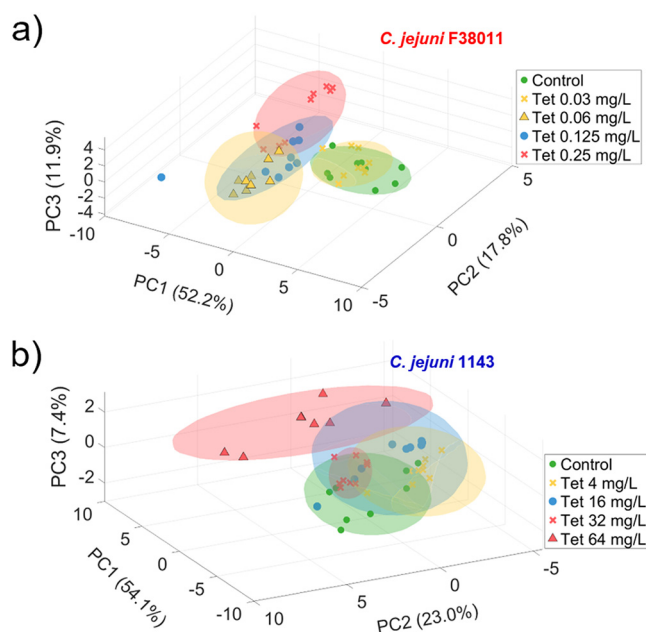
FIG 2 Determination of tetracycline MICs for *C. jejuni* using Raman spectroscopy-PCA. (a) PCA score plot associated with a susceptible isolate, *C. jejuni* F38011, after treatments with tetracycline concentrations of 0, 0.03, 0.06, 0.125, and 0.25 mg/liter. (b) PCA score plot for the resistant isolate *C. jejuni* 1143 after treatments with tetracycline concentrations of 0, 4, 16, 32, and 64 mg/liter. Colored shading is used as a visual aid to illustrate the clusters of each group. It was calculated as the mean $\pm$ 2 standard deviations, representing a confidence limit of 95%. The MIC in the Raman-PCA method is defined as the lowest antibiotic concentration that induces Raman spectral changes compared to the positive-control group (i.e., green cluster). The MICs determined by Raman-PCA were 0.06 mg/liter and 64 mg/liter, respectively.

equal or 2-fold higher values (Table 1). Similar results were reported in a previous study of clinical *E. coli* isolates (39). The authors proposed that multiple AMR mechanisms (e. g., more efflux pumps to extrude antibiotics) contribute to slower responses of bacterial strains resistant to antibiotic treatments, resulting in less significant alterations in Raman spectral features (39).

To further enhance the sensitivity of the Raman-based approach, we carried out a second-derivative transformation analysis to amplify minor spectral alterations and, thus, compensated for the potentially slower responses in the resistant strains. When a Raman peak responds to the antibiotic treatment, its inflection point (i.e., second derivative = 0) in the plot of Raman intensity versus antibiotic concentration indicates the antibiotic concentration that causes the maximal rate of Raman signal variation (i.e., the first-derivative Raman signal is a local maximum or local minimum). Figure 3 shows the second derivative of the Raman spectra with respect to the antibiotic concentrations. Regions with a positive second derivative (red color) indicate that Raman intensity is concave upward, while a negative second derivative (blue color) indicates that Raman intensity is concave downward. The averaged values of the inflection points over the region between 400 cm^{-1} and 1,800 cm^{-1} are marked by a black solid line in Fig. 3, and their values are summarized in Table 1. We found that the averaged inflection points agreed with the MICs determined by the agar dilution method within a 2-fold difference. In other words, essential agreement was achieved between the Raman-2nd derivative method and the agar dilution method for all the tested strains (38). Taken together, our studies demonstrated that the Raman-2nd derivative transformation analysis potentially provides an alternative method to determine the MICs for *C. jejuni*.

Antibiotic susceptibility profiles of *C. jejuni* determined by Raman-HCA. To improve the analysis throughput, we further explored if the Raman-based metabolomic approach could directly identify bacterial AMR categories without exposing bacteria to

TABLE 1 Summary of MICs in *Campylobacter jejuni* strains by the reference agar dilution method and Raman-chemometric methods

Antibiotic	Strain	Isolation source	AMR profile[a]	MIC (mg/liter)		
				Agar dilution	Raman-PCA[b]	Raman-2nd derivative
Ampicillin	F38011	Clinical	S	2	1	2
	1463	Quail	R	64	256*	32
Tetracycline	F38011	Clinical	S	0.125	0.06	0.06
	1143	Chicken	R	16	64*	16

[a]AMR profile was determined by the agar dilution method according to the protocol of the CLSI (60). The MIC breakpoints for ampicillin-susceptible (S) and -resistant (R) strains are 8 and 32 mg/liter, respectively (59). The MIC breakpoints for tetracycline-susceptible and -resistant strains are 4 and 16 mg/liter, respectively (60).
[b]Essential agreement is a critical indicator to verify the performance of a new approach. Essential agreement is achieved when MIC values obtained from the reference method and the newly developed approach are the same or within a 2-fold difference (38). The MIC values marked with an asterisk indicate that essential agreement was not achieved between the reference method and Raman spectroscopic-chemometric method. In other words, MICs determined by two methods were above a 2-fold dilution range.

serial 2-fold-diluted antibiotics. Instead of testing bacterial MICs with a wide range of antibiotic concentrations, we incubated *C. jejuni* with antibiotics at CLSI susceptible and resistant breakpoints. Bacterial samples in the absence of antibiotics were used as a positive control. Hierarchical clustering analysis (HCA) was performed to calculate the dissimilarity among sample groups. A susceptible strain is defined if all spectral replicates ($n = 9$) within the positive-control group are closely clustered and separated from both antibiotic treatment groups (i.e., MIC less than or equal to the CLSI susceptible breakpoint). On the other hand, a strain is defined as resistant if the spectra overlap (i.e., MIC
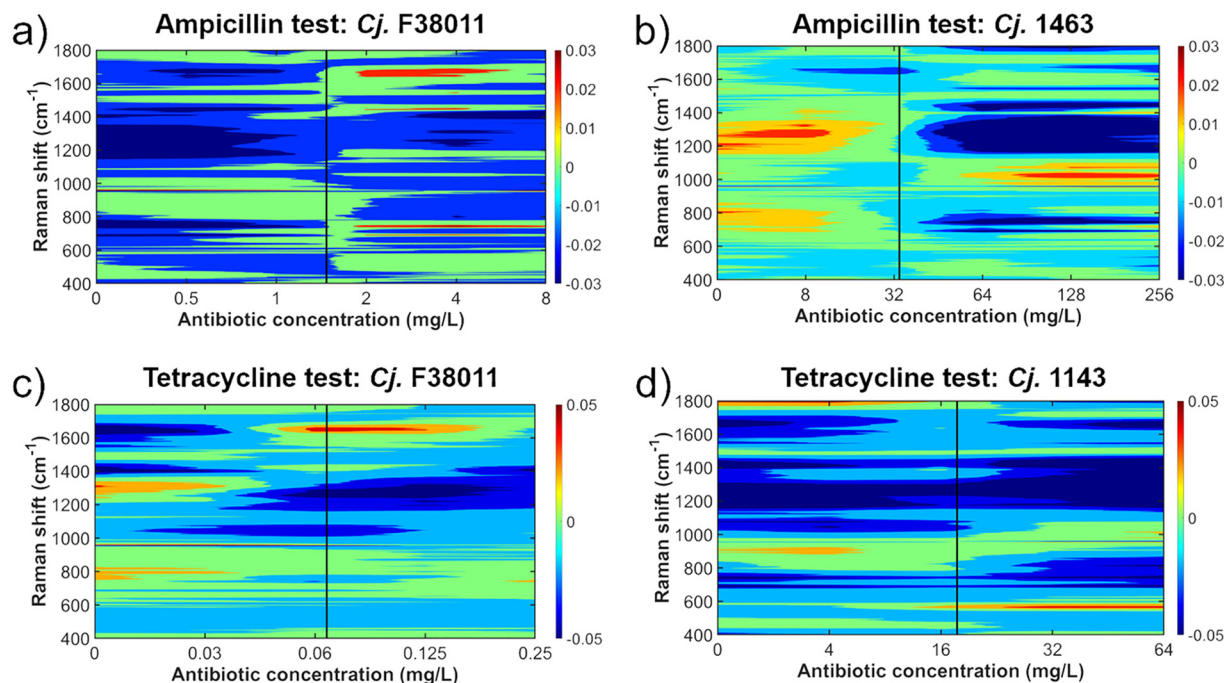

FIG 3 Determining the MICs in *C. jejuni* using Raman spectroscopy-2nd derivative transformation analysis. (a) Ampicillin test for susceptible isolate *C. jejuni* F38011; (b) ampicillin test for resistant isolate *C. jejuni* 1463; (c) tetracycline test for susceptible isolate *C. jejuni* F38011; (d) tetracycline test for resistant isolate *C. jejuni* 1143. The intensity in the color map represents the second-derivative values of Raman spectral intensity with respect to the antibiotic concentration. Regions with a positive second derivative (red color) indicate that the Raman intensity is concave upward; regions with a negative second derivative (blue color) indicate that the Raman intensity is concave downward; and second derivative at a value of 0 (green color) indicates an infection point, where the Raman intensity change reaches either local maximum or local minimum. The vertical black lines show the averaged values of the infection points over the whole spectral region (400 to 1,800 cm^{-1}). This averaged concentration was rounded up to the closest labeled antibiotic concentration and reported as the MIC obtained from Raman-2nd derivative transformation analysis.
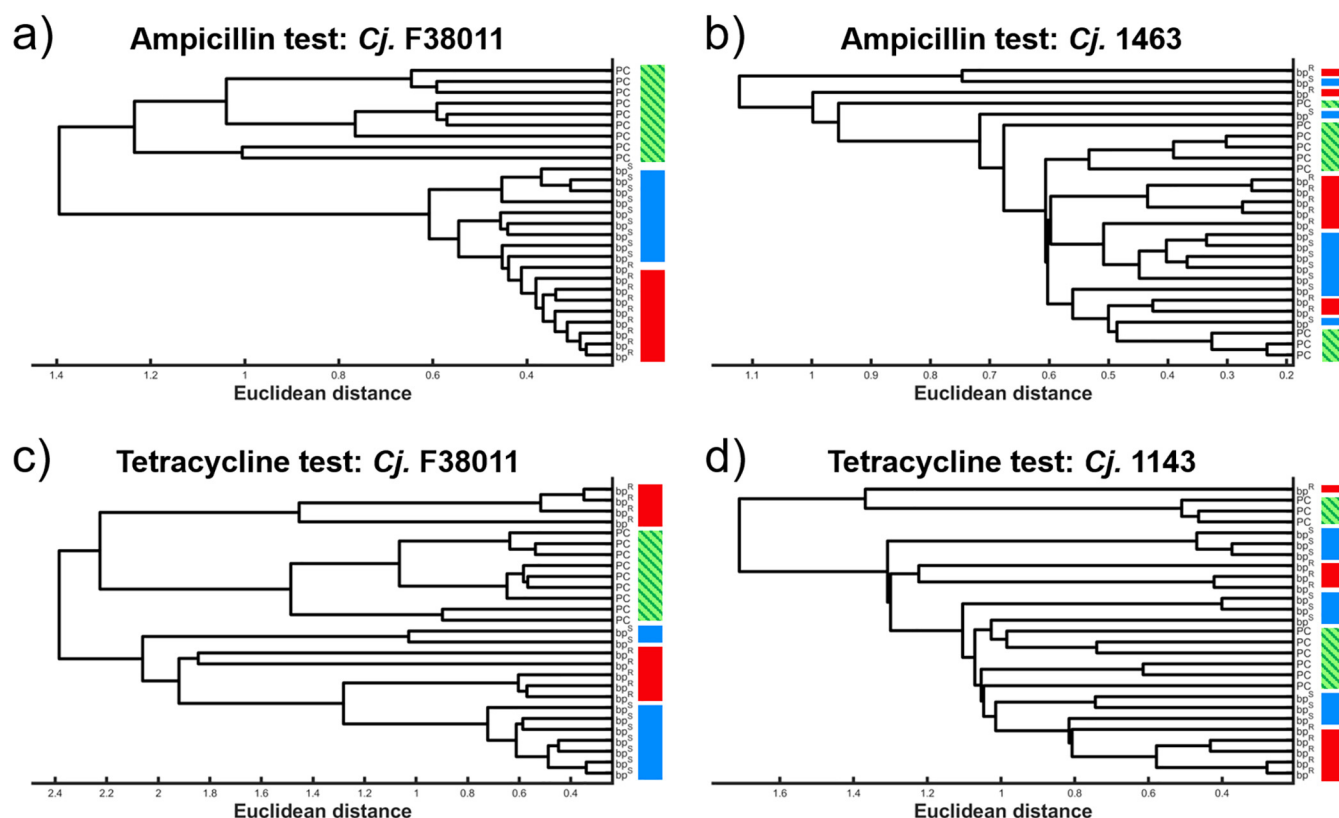
FIG 4 Hierarchical cluster analysis (HCA) for the determination for antibiotic susceptibility profiles for *C. jejuni*. (a) Ampicillin test for susceptible isolate *C. jejuni* F38011; (b) ampicillin test for resistant isolate *C. jejuni* 1463; (c) tetracycline test for susceptible isolate *C. jejuni* F38011; (d) tetracycline test for resistant isolate *C. jejuni* 1143. Samples labeled with PC, bp^S, and bp^R represent antibiotic treatments at concentrations of 0 mg/liter (green bar with a diagonal strip pattern), CLSI susceptible breakpoint (blue bar), and CLSI resistant breakpoint (red bar), respectively. Each treatment group had 9 replicates of Raman spectra. The Euclidean distance between each pair of spectra was calculated and used as the criterion to determine the spectral dissimilarity. A shorter Euclidean distance indicates a higher level of similarity. In the HCA-Raman method, *C. jejuni* isolates were regarded as susceptible strains if the untreated group (green bar with a diagonal strip pattern) clustered together but were separated from the antibiotic-treated samples (blue and red bars), while resistant strains were defined if all treatment groups were mixed together.

greater than or equal to the CLSI resistant breakpoint). The HCA dendrograms showed clear segregation of the untreated and treated groups for ampicillin- and tetracycline-susceptible strain F38011 (Fig. 4a and c), leading to correct classification for the susceptible strain. For *C. jejuni* 1463 and 1143, the dissimilarities (i.e., Euclidean distances) between the groups (i.e., cells treated at 0 mg/liter, CLSI susceptible breakpoint, and CLSI resistant breakpoint) were lower than those of within-group counterparts (Fig. 4b and d). This result indicated that both *C. jejuni* 1463 and *C. jejuni* 1143 were regarded as resistant strains by the Raman-HCA method, which agreed with the AMR profiles determined by the conventional agar dilution method (Table 1). Therefore, Raman-HCA is a promising tool for determining the AMR categories of *C. jejuni* strains.

AMR mechanisms revealed by Raman signatures. Besides rapid diagnostics of AMR pathogens, understanding the AMR mechanisms is of great importance to combating the AMR crisis, because they may provide insights for drug development and intervention measures. We implemented PCA loading plots to extract specific Raman peaks that were attributed to the differentiation of antibiotic-susceptible and -resistant *C. jejuni* strains. Briefly, PCA was performed for Raman spectra that were collected from the nontreated group as well as bacteria treated with antibiotics at CLSI susceptible and resistant breakpoints. We first assessed if there were any differences between Raman spectral features collected from susceptible and resistant strains after the same antibiotic treatment. According to the PCA score plots (Fig. 5a and b), similar results were identified for both ampicillin and tetracycline tests. After incubation at CLSI
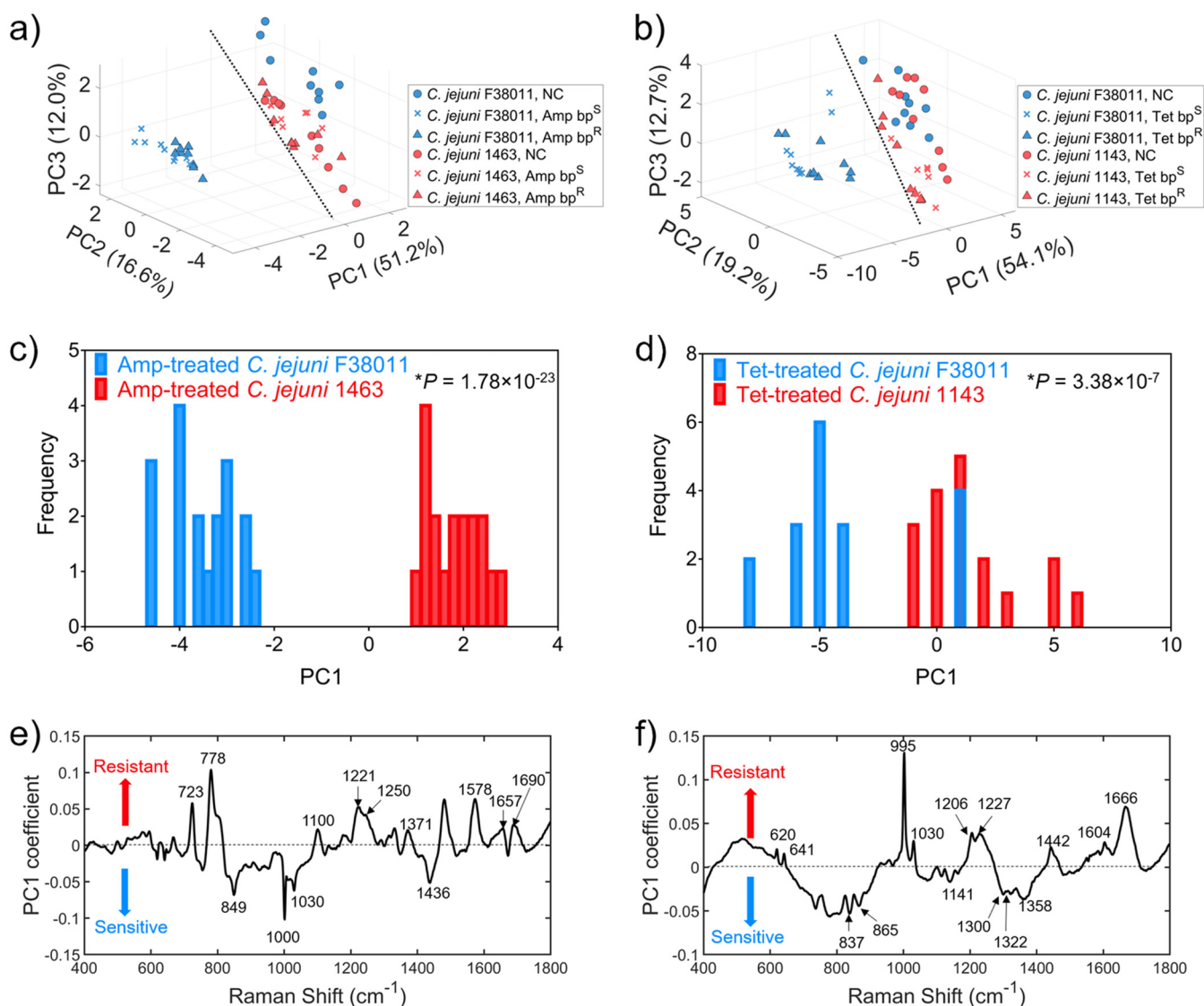
FIG 5 Principal-component analysis (PCA) for distinguishing resistant *C. jejuni* strains from susceptible strains ($n = 9$). Three-dimensional PCA score plots for the ampicillin (a) and tetracycline (b) studies are shown. Both susceptible (in blue) and resistant (in red) strains were treated with defined antibiotics at 0 mg/liter (negative control; NC), the CLSI susceptible breakpoint (bp^S), and the CLSI resistant breakpoint (bp^R). In panels a and b, black dotted lines indicate the separate clusters of susceptible and resistant strains after a 5-h antibiotic treatment, demonstrating the successful differentiation between susceptible and resistant strains. Histogram plots were constructed to demonstrate the distribution of ampicillin-treated strains (c) and tetracycline-treated strains (d) along with principal component 1 (PC1). Student's *t* test was carried out to determine the statistical difference between PC1 scores of antibiotic-treated susceptible strains and resistant strains (*, $P < 0.001$). Loading plots of PC1 for ampicillin test and tetracycline test are shown in panels e and f, respectively.

susceptible and resistant breakpoints for 5 h, the antibiotic-susceptible strain (F38011) formed a tight cluster and separated from the antibiotic-resistant strains (1463 and 1143) (Fig. 5a and b), indicating that different physiological behaviors existed in these two types of strains, as determined by the Raman-based approach. Meanwhile, an overlap was observed between the clusters of susceptible and resistant strains if they were not treated with any antibiotics (Fig. 5a and b). Thus, the differentiation between susceptible and resistant strains was attributed to bacterial responses against antibiotics rather than their natural biochemical compositions. Raman spectroscopy has shown its ability to discriminate the phenotypic diversity of *Campylobacter* at the species level (40–42), but to our knowledge, no studies have yet focused on strain-level diversity. Although the original phenotypic differences at the strain level might be negligible (Fig. 5a and b), future studies need to be performed to confirm if the Raman-chemometric approach can be applied to a more diverse range of *C. jejuni* strains.

TABLE 2 Molecular assignments of representative Raman peaks associated with ampicillin resistance mechanisms determined by Raman spectroscopy-based metabolomic approach

Wavenumber (cm^{-1})	Tentative peak assignment	Content	Reference(s)
723	Adenine ring breathing	Nucleic acid	47
778	Uracil, cytosine, thymine	Nucleic acid	34
849	Guanine, valine	Protein	33
1,000	Phenylalanine ring breathing	Protein	47
1,030	Phenylalanine, tyrosine	Protein	47
1,100	Symmetric phosphate stretching	Nucleic acid	47
1,221	CH bending in lipid	Lipid	47
1,250	Amide III	Protein	49
1,371	Pyruvate	Carbohydrate	33
1,436	Arginine	Protein	33
1,578	C-O vibration mode of peptidoglycan/ring stretching mode of adenine and guanine	Peptidoglycan/nucleic acid	44, 45
1,657	C=C stretching	Unsaturated fatty acid/lipid	47
1,690	Cytosine/amide I	Nucleic acid/protein	33, 50

Interestingly, a trend with increased resistance in *C. jejuni* could be observed along with an increase in PC1, which explained more than 50% of the total spectral variances in the data set (Fig. 5a to d). Ampicillin-treated susceptible and resistant strains were distributed at the negative and positive values of PC1, respectively (Fig. 5c). In the tetracycline treatment (Fig. 5d), 14 out of 18 Raman spectra that were collected from the tetracycline-treated susceptible strain F38011 showed lower PC1 scores than the resistant strain 1143. Regardless of antibiotic class, a significant difference ($P < 0.001$, Student's *t* test) was identified between PC1 scores obtained from antibiotic-treated susceptible and resistant strains (Fig. 5c and d). Since PC1 was positively correlated with a bacterial AMR profile, we constructed PC1 loading plots to extract specific Raman shifts that contributed to bacterial resistance. In Fig. 5e and f, maxima highlighted Raman peaks that were more pronounced in resistant strains, whereas minima depicted Raman peaks that were more associated with susceptible strains. Loading plots of the ampicillin and tetracycline tests exhibited different patterns (Fig. 5e and Fig. 5f), suggesting that the corresponding resistant strains employed distinctive resistant mechanisms. Tentative Raman peak assignments are listed in Tables 2 and 3 for ampicillin and tetracycline tests, respectively.

Ampicillin is one of the β-lactam antibiotics, which inhibit bacterial cell wall synthesis. This drug binds to penicillin-binding proteins in the inner membrane of the bacterial cell wall and interrupts the cross-linkage of peptidoglycan chains (43). As a result, the newly synthesized bacterial cell wall is no longer cross-linked and cannot maintain its strength and rigidity, eventually resulting in cell lysis. To survive under antibiotic stress, ampicillin-resistant strains are expected to have advanced strategies to maintain their cell envelopes. As shown in Fig. 5e, the peak at 1,578 cm^{-1} had a relatively large and positive PC1 coefficient, indicating its weighting in PC1. Previous studies demonstrated that the peak at 1,578 cm^{-1} might have contributions from both the ring modes of nucleic acids (44) and the C-O mode of peptidoglycan (45, 46). Berezin and coauthors used tip-enhanced Raman spectroscopy (TERS) to study the composition of bacterial cell walls and identified an enhanced Raman signal at 1,578 cm^{-1} when the TERS tip was localized at the cell wall (46). These results were consistent with the current study, indicating that a higher PC1 coefficient at 1,578 cm^{-1} for ampicillin-resistant strain 1463 than that of susceptible strain F38011 is due to a stronger formation of peptidoglycan in the *C. jejuni* cell wall. Lipid-associated peaks at 1,221 cm^{-1} and 1,657 cm^{-1} also had positive PC1 correlation coefficients (Fig. 5e), indicating that more lipid components are present in the cell envelope of the ampicillin-resistant strain than in the cell envelope of the susceptible strain (33, 47). Moreover, the PC1 coefficient at 1,221 cm^{-1} (CH bending mode in lipid) was about 2-fold higher than that at 1,657 cm^{-1} (C=C stretching mode in lipid), as shown in Fig. 5e. A higher PC1 coefficient represents a more prominent change in bacterial composition. In this case, we speculated

TABLE 3 Molecular assignments of representative Raman peaks associated with tetracycline resistance mechanisms determined by Raman spectroscopy-based metabolomic approach

Wavenumber (cm^{-1})	Tentative peak assignment	Content	Reference
620	C-C twisting of tryptophan	Protein	45
641	C-S stretching, C-C twisting of tyrosine	Protein	54
837	Tyrosine	Protein	58
865	Tryptophan	Protein	33
995	Phenylalanine	Protein	35
1,030	Tyrosine, phenylalanine	Protein	47
1,206	N-Acetylglucosamine	Cell wall	33
1,227	Adenine, thymine	Nucleic acid	47
	Amide III	Protein	
1,300	CH$_2$ deformation	Protein	54
1,322	C-N, N-H stretching in amide III, CH$_2$, CH$_3$ deformation	Protein	45
1,358	Adenine, glycine	Nucleic acid	47
	CH deformation	Protein	
1,442	Glycine	Protein	33
1,604	Phenylalanine	Protein	54
1,666	Amide I	Protein	49

that the ratio of saturated to unsaturated fatty acids potentially increased in the cell membranes of ampicillin-resistant strains, leading to a more rigid membrane structure. The alterations in membrane composition were previously reported as one of the most important adaptive mechanisms in bacteria when exposed to toxic compounds (48). Bacteria tend to increase the saturation level (i.e., rigidification) of membrane phospholipids so that less-toxic compounds can penetrate through the cell membrane. Furthermore, a shoulder peak at 1,250 cm^{-1} and a peak at 1,690 cm^{-1} (Fig. 5e) are possibly attributed to the amide III band and amide I band of proteins, respectively (49, 50). It is well-known that overexpression of cmeABC-encoded efflux pumps on cell membranes plays a critical role in multidrug resistance of C. jejuni (16, 43). This might explain the increased protein content in the ampicillin-resistant strain 1463. Most of the other positive peaks potentially are associated with nucleic acids (723, 778, 1,100, and 1,690 cm^{-1}) and pyruvate (1,371 cm^{-1}), which are regarded as indicators of active bacterial growth (33, 34, 39, 47, 51). On the other hand, negative peaks at 849, 1,000, 1,030, and 1,436 cm^{-1} are all related to amino acids and proteins, as shown in Fig. 5e (33, 47). The negative PC1 coefficients implied that larger amounts of amino acids and proteins are accumulated in ampicillin-sensitive strains than in resistant strains. The enhanced synthesis of amino acids and proteins in ampicillin-susceptible strain F38011 might reflect bacterial stress responses to adverse conditions (e.g., ampicillin treatment) (52).

Raman spectra suggested that the tetracycline resistance of C. jejuni is related to the protein inhibitory effect and cell envelope integrity. Tetracyclines are widely used for humans and animals due to their broad-spectrum antimicrobial effect targeting both Gram-negative and Gram-positive bacteria (53). Tetracyclines can reversibly inhibit protein synthesis by preventing the association between aminoacyl-tRNA and the 30S subunit of ribosomes. In this study, our results suggested that tetracycline resistance was related to protein and nucleic acid synthesis. In Fig. 5f, most prominent peaks with positive PC1 coefficients are associated with proteins, including phenylalanine (995, 1,030, 1,604 cm^{-1}), amide I band (1,666 cm^{-1}), amide III band (1,227 cm^{-1}), tryptophan (620 cm^{-1}), and tyrosine (641 cm^{-1}) (35, 45, 47, 49, 54). The higher level of proteins in tetracycline-resistant strain 1143 suggested a reduced protein inhibitory effect of tetracycline. According to previous studies, two major resistance mechanisms contribute to tetracycline resistance in Campylobacter, namely, antimicrobial extrusion by efflux pumps and the synthesis of ribosomal protection protein TetO (14, 53, 55). Both mechanisms involved protein-based bacterial structures (e.g., CmeABC efflux pump and TetO) that may contribute to the relatively high intensity of protein-related Raman peaks in the tetracycline-resistant strain 1143. A previous study observed an increase

of amide III in tetracycline-treated *E. coli* by using infrared spectroscopy, and the authors linked this effect to enhanced synthesis of transport proteins, such as efflux pumps (35). Additionally, our study showed that the peak at 1,206 cm^{-1} exhibited a positive PC1 coefficient (Fig. 5f). This peak can be assigned to *N*-acetylglucosamine, which is the building block of a bacterial cell wall (33). The relatively high cell wall content suggested that AMR is related to proper protein synthesis and cell envelope integrity in the tetracycline-resistant strain 1143. Athamneh and others reported similar results for *E. coli*, in which tetracycline treatment influenced both cell walls and protein synthesis (56). Our results suggested that nucleic acid-related peaks (thymine, adenine, 1,227 cm^{-1}; glycine, 1,442 cm^{-1}) were positively related to tetracycline resistance (Fig. 5f) (33). Our results were in good agreement with the mode of action of tetracycline. As for the secondary consequence of protein synthesis inhibition by tetracycline, the initiation of new rounds of DNA synthesis would be interrupted due to the lack of necessary enzymes (57). In other words, tetracycline-resistant strains could have faster DNA synthesis and, thus, more DNA content than susceptible strains when treated with tetracycline. We also found several negative peaks that were related to proteins (837, 865, 1,300, 1,322, and 1,358 cm^{-1}) and nucleic acids (1,358 cm^{-1}) (33, 45, 47, 54, 58), indicating that tetracycline-susceptible strain F38011 undergoes stress responses to combat the inhibitory effects from tetracycline.

Conclusions. We developed a Raman-based metabolomic approach to determine the MICs of antibiotics and AMR profiles for *Campylobacter*. When a *C. jejuni* isolate is treated with antibiotics, its Raman spectra reveal the alteration of biochemical features along with the change of antibiotic concentrations. As a result, the MICs or antimicrobial susceptibilities for *C. jejuni* can be determined by comparing Raman spectra of the positive-control and treated groups without requirements for predeveloped models or databases. The analysis can be completed within ~5 h, which is superior to the conventional culture-based method, especially for fastidious and slow-growing bacteria. This high-throughput AST method has the potential to identify multidrug-resistant pathogens for timely diagnostics and medical prescriptions in health care settings. Future studies will be conducted to further investigate the feasibility of Raman-chemometric approaches for a diverse range of *C. jejuni* isolates as well as different antibiotic classes (e.g., macrolides and fluoroquinolones) that are listed in the current AMR surveillance systems (32). Furthermore, AMR mechanisms of *Campylobacter* were deciphered based on the rich biochemical information in the Raman metabolomic data. The knowledge obtained from this study provides insights into AMR mechanisms that can be used to develop either novel antimicrobials or combinational applications of current antibiotics for synergetic antimicrobial effects.

MATERIALS AND METHODS

Antibiotics. Ampicillin sodium salt (purity, 95%) and tetracycline hydrochloride (purity, 98%) were purchased from Millipore Sigma. Antibiotic stock solutions (6,400 mg/liter) were prepared in distilled water and filtrated through 0.2-μm polyethersulfone (PES) syringe filters. Aliquots of sterilized antibiotic solution were stored at −20°C and freshly thawed for individual experimental days.

Bacterial strains and cultivation conditions. *C. jejuni* strains F38011 (clinical isolate), 1143 (chicken isolate), and 1463 (quail isolate) were used due to their distinct antimicrobial susceptibility profiles (Table 1). Bacterial isolates were preserved at −80°C in cryogenic culture medium containing 20% glycerol, 10% defibrinated sheep blood, and 70% bacterial culture in Mueller-Hinton broth (MHB; BD Difco). For each independent experiment, a fresh bacterial culture was prepared by streaking ~50 μl of bacterial glycerol stock onto Mueller-Hinton II agar plates (BD) supplemented with 5% defibrinated sheep blood (MHBA). The incubation was performed at 37°C under microaerobic conditions for 48 h. Several *C. jejuni* colonies on MHBA were then transferred into MHB and incubated at 37°C with constant shaking (175 rpm) under microaerobic conditions. After cultivation for 16 h, overnight culture reached late log phase for antibiotic tests.

MIC determination by the standard culture-based method. MICs of antibiotics for *C. jejuni* were determined by the agar dilution method as described by the CLSI guidelines (59, 60). Bacterial AMR profiles (i.e., susceptible or resistant) were determined based on CLSI breakpoints. As no ampicillin breakpoints are available for *Campylobacter*, we used the breakpoints for *Enterobacteriaceae* instead (59, 60). The results were used to validate the accuracy of MICs and AMR profiles obtained by the Raman-based AST.

Sample preparation for Raman-based AST. Serial 2-fold dilutions of antibiotics (4 ml) were prepared with MHB. Table S1 in the supplemental material summarizes the details of tested antibiotic concentrations, which were dependent on the type of antibiotics and AMR profiles of *C. jejuni* isolates. Overnight culture of *C. jejuni* was diluted to an optical density at 600 nm (OD_{600}) of 0.06 (equivalent to 2×10^8 CFU/ml), and an aliquot (4 ml) was mixed with defined concentrations of an antibiotic. Bacterial culture without exposure to any antibiotics was considered the positive control. Each inoculated culture was incubated for 5 h at 37°C with shaking at 175 rpm under microaerobic conditions. To monitor the antibiotic inhibitory effect, viable bacterial cells were enumerated using the plating assay (61). Briefly, bacterial samples were 10-fold serially diluted in $1\times$ phosphate-buffered saline buffer (pH 7.4), and 10-μl aliquots were streaked on MHBA plates. The MHBA plates were incubated at 37°C under microaerobic conditions for 48 h. Following the incubation, colony numbers were counted and reported as the number of CFU per milliliter.

After antibiotic treatment, samples were harvested by centrifugation at 15,000 $\times$ *g* for 3 min. The supernatant was discarded, and the remaining bacterial pellet was washed with sterile distilled water three times to remove potentially interfering substances. The washed bacterial pellet was resuspended in distilled water. For Raman spectral acquisition, 2 μl of bacterial suspension was deposited onto a commercial gold-coated microarray glass slide (BioGold; Thermo Fisher Scientific). This gold-coated glass slide was selected as the Raman substrate because it effectively reduces the fluorescence background from glass and barely contributes to the collected Raman spectra of bacterial samples (62, 63).

Raman spectral acquisition. Raman spectra were collected using a confocal Raman microscope (inVia; Renishaw) coupled to a spectrograph with a grating of 1,200 lines/mm and a charge-coupled device (CCD) array detector with 578 by 385 pixels. A 785-nm laser (Renishaw) served as the excitation source with an incident laser power of 15 mW. A $50\times$ lens objective (numerical aperture, 0.75; Leica) was used to focus the laser beam on bacterial samples and collect the backscattered Raman signal. The scattered light was filtered by a long-pass filter before it entered the spectrograph and CCD. The spectral resolution was 0.8 cm^{-1}. The wavenumber was calibrated using a silicon Raman peak at 520 cm^{-1} to ensure an accuracy of ± 1 cm^{-1}. Raman spectra were collected over the wavenumber region of 400 to 1,800 cm^{-1}. To obtain the desired signal-to-noise ratio, each Raman spectrum was acquired in 60 s. Three Raman spectra were randomly collected from different spots of each bacterial sample, and the experiment was independently conducted in triplicate, resulting in 9 individual spectra per treatment group.

Spectral preprocessing and chemometric analyses. Spectral preprocessing included baseline removal, smoothing, and normalization. The Vancouver Raman Algorithm v1.0.0 with a fifth-order polynomial fitting was applied to all Raman spectra to remove the background signal caused by intrinsic fluorescence (64, 65). Spectra were smoothed on OMNIC spectroscopy software (Thermo Fisher Scientific) using a Savitzki-Golay filter with a 5-point-wide window and a 2nd-order polynomial fit. To reduce the variation of cell density in bacterial samples, spectra were normalized against a Raman peak at 1,002 cm^{-1}, which is attributed to the ring breathing mode of phenylalanine (34). Normalization and the subsequent chemometric analyses were completed on MATLAB version R2018b (The MathWorks, Inc.).

To determine the MICs for tested *C. jejuni* isolates, we carried out two chemometric methods, namely, principal-component analysis (PCA) and second-derivative transformation analysis, on the preprocessed and untransformed Raman spectra in the wavenumber range of 400 to 1,800 cm^{-1}. First, PCA was used to distinguish the spectra from untreated and treated bacterial cells as a function of antibiotic concentration. Three-dimensional (3D) PCA score plots were constructed to visualize the similarities and differences between spectra. The MIC of an antibiotic for *C. jejuni* in the Raman-PCA method is defined as the lowest antibiotic concentration that induces Raman spectral changes compared to the positive-control group (i.e., a separate cluster away from the positive-control group). The cluster of each group was drawn based on the mean $\pm$ 2 standard deviations, representing a confidence level of 95%. If two clusters are not overlapping, they are regarded as significantly different groups ($P < 0.05$). In parallel, second-derivative transformation analyses were performed on the preprocessed Raman spectra to identify spectral differences between antibiotic treatment groups. At each Raman shift, second-derivative transformation was applied to Raman intensity as a function of antibiotic concentration. When the second-derivative-transformed Raman intensity equaled 0 (i.e., the infection point), we recorded the corresponding antibiotic concentration for each Raman shift. Since the MIC reflects the overall profile (i.e., population level) of a bacterial response to antibiotic treatment, we averaged the antibiotic concentrations at infection points from all Raman shifts (400 to 1,800 cm^{-1}) and regarded that average as a Raman-based MIC value.

Hierarchical cluster analysis (HCA) was employed to classify the AMR profiles of *C. jejuni* isolates to be either susceptible or resistant (26). We analyzed Raman spectra collected from three antibiotic treatment groups, namely, untreated cells, cells treated at the CLSI susceptible breakpoint of antibiotics, and cells treated at the CLSI resistant breakpoint of antibiotics. The Euclidean distance between each pair of spectra was calculated and used as the criteria to determine the spectral dissimilarity. The single clustering algorithm was used to split samples into various hierarchical clusters based on their spectral distances. A dendrogram was generated to visualize spectral classification, where similar spectra would be grouped into the neighboring branches. As a result, a susceptible strain was identified if the spectra of untreated and treated groups were divided into two clusters, while a resistant strain was one whose spectra from all three groups were interlaced.

To further investigate the molecule-based mechanisms of *C. jejuni* AMR using the Raman-based metabolomic approach, we performed PCA on the preprocessed and untransformed spectra from both susceptible and resistant isolates with and without antibiotics. Histogram plots were presented to visualize the distribution of Raman spectra along principal components (PCs). Loading plots of principal

components were created to identify the Raman shifts that indicate spectral variances between suscepti-ble and resistant strains.

Statistical analysis. To demonstrate the typical Raman spectral pattern and reproducibility, the mean $\pm$ standard deviation of Raman spectra were calculated. Student's t test (two-tailed) was per-formed to assess the statistical difference between PC1 scores of the antibiotic-treated susceptible and resistant strains. One-way analysis of variance (ANOVA) followed by Games-Howell test was carried out to determine whether *C. jejuni* strains treated with a range of ampicillin concentrations showed signifi-cantly different Raman intensities at selected Raman bands. One-way ANOVA followed by Dunnett's test was used to determine statistical differences between bacterial cell counts of the positive-control and antibiotic-treated groups. The statistical significance threshold was set at 95% ($P < 0.05$).

SUPPLEMENTAL MATERIAL

Supplemental material is available online only.

SUPPLEMENTAL FILE 1, PDF file, 0.3 MB.

REFERENCES

1. European Food Safety Authority, European Centre for Disease Prevention and Control. 2019. The European Union One Health 2018 zoonoses report. EFSA J 17:e05926. https://doi.org/10.2903/j.efsa.2019.5926.
2. Tack DM, Marder EP, Griffin PM, Cieslak PR, Dunn J, Hurd S, Scallan E, Lathrop S, Muse A, Ryan P, Smith K, Tobin D, Angelo M, Vugia DJ, Hk G, Wolpert BJ, Tauxe R, Geissler AL. 2019. Preliminary incidence and trends of infections with pathogens transmitted commonly through food–food-borne diseases active surveillance network, 10 U.S. sites, 2015. Am J Transplant 19:1859–1863. https://doi.org/10.1111/ajt.15412.
3. Silva J, Leite D, Fernandes M, Mena C, Gibbs PA, Teixeira P. 2011. Campy-lobacter spp. as a foodborne pathogen: a review. Front Microbiol 2:200–211. https://doi.org/10.3389/fmicb.2011.00200.
4. Kaakoush NO, Castaño-Rodríguez N, Mitchell HM, Man SM. 2015. Global epidemiology of Campylobacter infection. Clin Microbiol Rev 28:687–720. https://doi.org/10.1128/CMR.00006-15.
5. Centers for Disease Control and Prevention (CDC). 2013 Antibiotic resist-ance threats in the United States, 2013. CDC, Atlanta, GA.
6. Smith KE, Besser JM, Hedberg CW, Leano FT, Bender JB, Wicklund JH, Johnson BP, Moore KA, Osterholm MT. 1999. Quinolone-resistant Campy-lobacter jejuni infections in Minnesota, 1992–1998. N Engl J Med 340:1525–1532. https://doi.org/10.1056/NEJM199905203402001.
7. Ge B, Wang F, Sjölund-Karlsson M, McDermott PF. 2013. Antimicrobial re-sistance in Campylobacter: susceptibility testing methods and resistance trends. J Microbiol Methods 95:57–67. https://doi.org/10.1016/j.mimet.2013.06.021.
8. Moore JE, Barton MD, Blair IS, Corcoran D, Dooley JSG, Fanning S, Kempf I, Lastovica AJ, Lowery CJ, Matsuda M, McDowell DA, McMahon A, Millar BC, Rao JR, Rooney PJ, Seal BS, Snelling WJ, Tolba O. 2006. The epidemiology of antibiotic resistance in Campylobacter. Microbes Infect 8:1955–1966. https://doi.org/10.1016/j.micinf.2005.12.030.
9. Paphitou NI. 2013. Antimicrobial resistance: action to combat the rising microbial challenges. Int J Antimicrob Agents 42:S25–S28. https://doi.org/10.1016/j.ijantimicag.2013.04.007.
10. Tornimbene B, Eremin S, Escher M, Griskeviciene J, Manglani S, Pessoa-Silva CL. 2018. WHO global antimicrobial resistance surveillance system early implementation 2016–17. Lancet Infect Dis 18:241–242. https://doi.org/10.1016/S1473-3099(18)30060-4.
11. Tacconelli E, Carrara E, Savoldi A, Harbarth S, Mendelson M, Monnet DL, Pulcini C, Kahlmeter G, Kluytmans J, Carmeli Y, Ouellette M, Outterson K, Patel J, Cavaleri M, Cox EM, Houchens CR, Grayson ML, Hansen P, Singh N, Theuretzbacher U, Magrini N, WHO Pathogens Priority List Working Group. 2018. Discovery, research, and development of new antibiotics: the WHO priority list of antibiotic-resistant bacteria and tuberculosis. Lancet Infect Dis 18:318–327. https://doi.org/10.1016/S1473-3099(17)30753-3.
12. Laws M, Shaaban A, Rahman KM. 2019. Antibiotic resistance breakers: cur-rent approaches and future directions. FEMS Microbiol Rev 43:490–516. https://doi.org/10.1093/femsre/fuz014.
13. Brown D. 2015. Antibiotic resistance breakers: can repurposed drugs fill the antibiotic discovery void? Nat Rev Drug Discov 14:821–832. https://doi.org/10.1038/nrd4675.
14. Gibreel A, Wetsch NM, Taylor DE. 2007. Contribution of the CmeABC efflux pump to macrolide and tetracycline resistance in Campylobacter jejuni. Antimicrob Agents Chemother 51:3212–3216. https://doi.org/10.1128/AAC.01592-06.
15. Han J, Sahin O, Barton YW, Zhang Q. 2008. Key role of Mfd in the develop-ment of fluoroquinolone resistance in Campylobacter jejuni. PLoS Pathog 4:e1000083-12. https://doi.org/10.1371/journal.ppat.1000083.
16. Lin J, Overbye Michel L, Zhang Q. 2002. CmeABC functions as a multidrug efflux system in Campylobacter jejuni. Antimicrob Agents Chemother 46:2124–2131. https://doi.org/10.1128/aac.46.7.2124-2131.2002.
17. Rokney A, Valinsky L, Vranckx K, Feldman N, Agmon V, Moran-Gilad J, Weinberger M. 2020. WGS-based prediction and analysis of antimicrobial resistance in Campylobacter jejuni isolates from Israel. Front Cell Infect Microbiol 10:365. https://doi.org/10.3389/fcimb.2020.00365.
18. Painset A, Day M, Doumith M, Rigby J, Jenkins C, Grant K, Dallman TJ, Godbole G, Swift C. 2020. Comparison of phenotypic and WGS-derived antimicrobial resistance profiles of Campylobacter jejuni and Campylo-bacter coli isolated from cases of diarrhoeal disease in England and Wales, 2015–16. J Antimicrob Chemother 75:883–889. https://doi.org/10.1093/jac/dkz539.
19. Ellington MJ, Ekelund O, Aarestrup FM, Canton R, Doumith M, Giske C, Grundman H, Hasman H, Holden MTG, Hopkins KL, Iredell J, Kahlmeter G, Köser CU, MacGowan A, Mevius D, Mulvey M, Naas T, Peto T, Rolain J-M, Samuelsen Ø, Woodford N. 2017. The role of whole genome sequencing in antimicrobial susceptibility testing of bacteria: report from the EUCAST subcommittee. Clin Microbiol Infect 23:2–22. https://doi.org/10.1016/j.cmi.2016.11.012.
20. Ho C-S, Jean N, Hogan CA, Blackmon L, Jeffrey SS, Holodniy M, Banaei N, Saleh AAE, Ermon S, Dionne J. 2019. Rapid identification of pathogenic bacteria using Raman spectroscopy and deep learning. Nat Commun 10:4927–4928. https://doi.org/10.1038/s41467-019-12898-9.

21. Rubakhin SS, Lanni EJ, Sweedler JV. 2013. Progress toward single cell metabolomics. Curr Opin Biotechnol 24:95–104. https://doi.org/10.1016/j.copbio.2012.10.021.

22. Premasiri WR, Lee JC, Sauer-Budge A, Théberge R, Costello CE, Ziegler LD. 2016. The biochemical origins of the surface-enhanced Raman spectra of bacteria: a metabolomics profiling by SERS. Anal Bioanal Chem 408:4631–4647. https://doi.org/10.1007/s00216-016-9540-x.

23. Xu J, Preciado-Llanes L, Aulicino A, Decker CM, Depke M, Gesell Salazar M, Schmidt F, Simmons A, Huang WE. 2019. Single-cell and time-resolved profiling of intracellular Salmonella metabolism in primary human cells. Anal Chem 91:7729–7737. https://doi.org/10.1021/acs.analchem.9b01010.

24. Hong W, Karanja CW, Abutaleb NS, Younis W, Zhang X, Seleem MN, Cheng JX. 2018. Antibiotic susceptibility determination within one cell cycle at single-bacterium level by stimulated Raman metabolic imaging. Anal Chem 90:3737–3743. https://doi.org/10.1021/acs.analchem.7b03382.

25. Ayala OD, Wakeman CA, Pence IJ, Gaddy JA, Slaughter JC, Skaar EP, Mahadevan-Jansen A. 2018. Drug-resistant Staphylococcus aureus strains reveal distinct biochemical features with Raman microspectroscopy. ACS Infect Dis 4:1197–1210. https://doi.org/10.1021/acsinfecdis.8b00029.

26. Lin Z, Zhao X, Huang J, Liu W, Zheng Y, Yang X, Zhang Y, Lamy De La Chapelle M, Fu W. 2019. Rapid screening of colistin-resistant: Escherichia coli, Acinetobacter baumannii and Pseudomonas aeruginosa by the use of Raman spectroscopy and hierarchical cluster analysis. Analyst 144:2803–2810. https://doi.org/10.1039/c8an02220h.

27. Lu X, Samuelson DR, Rasco BA, Konkel ME. 2012. Antimicrobial effect of diallyl sulphide on Campylobacter jejuni biofilms. J Antimicrob Chemother 67:1915–1926. https://doi.org/10.1093/jac/dks138.

28. Lu X, Rasco BA, Jabal JMFF, Eric Aston D, Lin M, Konkel ME, Aston DE, Lin M, Konkel ME. 2011. Investigating antibacterial effects of garlic (Allium sativum) concentrate and garlic-derived organosulfur compounds on Campylobacter jejuni by using fourier transform infrared spectroscopy, Raman spectroscopy, and electron microscopy. Appl Environ Microbiol 77:5257–5269. https://doi.org/10.1128/AEM.02845-10.

29. Lu X, Weakley AT, Aston DE, Rasco BA, Wang S, Konkel ME. 2012. Examination of nanoparticle inactivation of Campylobacter jejuni biofilms using infrared and Raman spectroscopies. J Appl Microbiol 113:952–963. https://doi.org/10.1111/j.1365-2672.2012.05373.x.

30. Xue R, Feng J, Ma L, Liu C, Xian M, Konkel ME, Wang S, Lu X. 2018. Whole transcriptome sequencing analysis of the synergistic antimicrobial effect of metal oxide nanoparticles and ajoene on Campylobacter jejuni. Front Microbiol 9:2074–2011. https://doi.org/10.3389/fmicb.2018.02074.

31. Windiasti G, Feng J, Ma L, Hu Y, Hakeem MJ, Amoako K, Delaquis P, Lu X. 2019. Investigating the synergistic antimicrobial effect of carvacrol and zinc oxide nanoparticles against Campylobacter jejuni. Food Control 96:39–46. https://doi.org/10.1016/j.foodcont.2018.08.028.

32. Goverment of Canada. 2018. Canadian Integrated Program for Antimicrobial Resistance Survillance (CIPARS) 2016 annual report. Public Health Agency of Canada, Guelph, Ontario, Canada. http://publications.gc.ca/collections/collection_2018/aspc-phac/HP2-4-2016-eng.pdf.

33. Kiefer W, Mazzolini AP, Stoddart PR. 2007. Reference database of Raman spectra of biological molecules. J Raman Spectrosc 38:1538–1553. https://doi.org/10.1002/jrs.1902.

34. Jung GB, Nam SW, Choi S, Lee G-J, Park H-K, Bok Jung G, Won Nam S, Choi S, Lee G-J, Park H-K, Jung GB, Nam SW, Choi S, Lee G-J, Park H-K. 2014. Evaluation of antibiotic effects on Pseudomonas aeruginosa biofilm using Raman spectroscopy and multivariate analysis. Biomed Opt Express 5:3238–3251. https://doi.org/10.1364/BOE.5.003238.

35. Xuan Nguyen NT, Sarter S, Hai Nguyen N, Daniel P. 2017. Detection of molecular changes induced by antibiotics in Escherichia coli using vibrational spectroscopy. Spectrochim Acta A Mol Biomol Spectrosc 183:395–401. https://doi.org/10.1016/j.saa.2017.04.077.

36. Wang P, Pang S, Zhang H, Fan M, He L. 2016. Characterization of Lactococcus lactis response to ampicillin and ciprofloxacin using surface-enhanced Raman spectroscopy. Anal Bioanal Chem 408:933–941. https://doi.org/10.1007/s00216-015-9184-2.

37. Lever J, Krzywinski M, Altman N. 2017. Principal component analysis. Nat Methods 14:641–642. https://doi.org/10.1038/nmeth.4346.

38. Humphries RM, Ambler J, Mitchell SL, Castanheira M, Dingle T, Hindler JA, Koeth L, Sei K, Hardy D, Zimmer B, Butler-Wu S, Dien Bard J, Brasso B, Shawar R, Dingle T, Humphries R, Sei K, Koeth L. 2018. CLSI methods development and standardization working group best practices for evaluation of antimicrobial susceptibility tests. J Clin Microbiol 56:e01934-17. https://doi.org/10.1128/JCM.01934-17.

39. Kirchhoff J, Glaser U, Bohnert JA, Pletz MW, Popp J, Neugebauer U. 2018. Simple ciprofloxacin resistance test and determination of minimal inhibitory concentration within 2 h using Raman spectroscopy. Anal Chem 90:1811–1818. https://doi.org/10.1021/acs.analchem.7b03800.

40. Read DS, Woodcock DJ, Strachan NJC, Forbes KJ, Colles FM, Maiden MCJ, Clifton-Hadley F, Ridley A, Vidal A, Rodgers J, Whiteley AS, Sheppard SK. 2013. Evidence for phenotypic plasticity among multihost Campylobacter jejuni and C. coli lineages, obtained using ribosomal multilocus sequence typing and Raman spectroscopy. Appl Environ Microbiol 79:965–973. https://doi.org/10.1128/AEM.02521-12.

41. Lu X, Huang Q, Miller WG, Aston DE, Xu J, Xue F, Zhang H, Rasco BA, Wang S, Konkel ME. 2012. Comprehensive detection and discrimination of Campylobacter species by use of confocal micro-Raman spectroscopy and multilocus sequence typing. J Clin Microbiol 50:2932–2946. https://doi.org/10.1128/JCM.01144-12.

42. Muhamadali H, Weaver D, Subaihi A, Almasoud N, Trivedi DK, Ellis DI, Linton D, Goodacre R. 2016. Chicken, beams, and Campylobacter: rapid differentiation of foodborne bacteria via vibrational spectroscopy and MALDI-mass spectrometry. Analyst 141:111–122. https://doi.org/10.1039/c5an01945a.

43. Wieczorek K, Osek J. 2013. Antimicrobial resistance mechanisms among Campylobacter. Biomed Res Int 2013:340605–340612. https://doi.org/10.1155/2013/340605.

44. Maquelin K, Kirschner C, Choo-Smith LP, Van Den Braak N, Endtz HP, Naumann D, Puppels GJ. 2002. Identification of medically relevant microorganisms by vibrational spectroscopy. J Microbiol Methods 51:255–271. https://doi.org/10.1016/s0167-7012(02)00127-6.

45. de Siqueira e Oliveira FS, Giana HE, Silveira L. 2012. Discrimination of selected species of pathogenic bacteria using near-infrared Raman spectroscopy and principal components analysis. J Biomed Opt 17:107004–107008. https://doi.org/10.1117/1.JBO.17.10.107004.

46. Berezin S, Aviv Y, Aviv H, Goldberg E, Tischler YR. 2017. Replacing a century old technique-modern spectroscopy can supplant Gram staining. Sci Rep 7:3810–3817. https://doi.org/10.1038/s41598-017-02212-2.

47. Germond A, Ichimura T, Horinouchi T, Fujita H, Furusawa C, Watanabe TM. 2018. Raman spectral signature reflects transcriptomic features of antibiotic resistance in Escherichia coli. Commun Biol 1:85–90. https://doi.org/10.1038/s42003-018-0093-8.

48. Murínová S, Dercová K. 2014. Response mechanisms of bacterial degraders to environmental contaminants on the level of cell walls and cytoplasmic membrane. Int J Microbiol 2014:873081–873096. https://doi.org/10.1155/2014/873081.

49. Huang WE, Griffiths RI, Thompson IP, Bailey MJ, Whiteley AS. 2004. Raman microscopic analysis of single microbial cells. Anal Chem 76:4452–4458. https://doi.org/10.1021/ac049753k.

50. Maiti NC, Apetri MM, Zagorski MG, Carey PR, Anderson VE. 2004. Raman spectroscopic characterization of secondary structure in natively unfolded proteins: α-synuclein. J Am Chem Soc 126:2399–2408. https://doi.org/10.1021/ja0356176.

51. Stahl M, Butcher J, Stintzi A. 2012. Nutrient acquisition and metabolism by Campylobacter jejuni. Front Cell Infect Microbiol 2:5. https://doi.org/10.3389/fcimb.2012.00005.

52. Tangwatcharin P, Chanthachum S, Khopaibool P, Griffiths MW. 2006. Morphological and physiological responses of Campylobacter jejuni to stress. J Food Prot 69:2747–2753. https://doi.org/10.4315/0362-028x-69.11.2747.

53. Chopra I, Roberts MM. 2001. Tetracycline antibiotics: mode of action, applications, molecular biology, and epidemiology of bacterial resistance. Microbiol Mol Biol Rev 65:232–260. https://doi.org/10.1128/MMBR.65.2.232-260.2001.

54. De Gelder J, De Gussem K, Vandenabeele P, Vancanneyt M, De Vos P, Moens L. 2007. Methods for extracting biochemical information from bacterial Raman spectra: focus on a group of structurally similar biomolecules-fatty acids. Anal Chim Acta 603:167–175. https://doi.org/10.1016/j.aca.2007.09.049.

55. Zhang Q, Plummer PJ. 2008. Mechanisms of antibiotic resistance in Campylobacter, p 263–276. In Szymanski CM, Blaser MJ, Nachamkin I (ed), Campylobacter, 3rd ed. American Society of Microbiology, Washington, DC.

56. Athamneh AIM, Alajlouni RA, Wallace RS, Seleem MN, Senger RS, Sengera RS. 2014. Phenotypic profiling of antibiotic response signatures in Escherichia coli using Raman spectroscopy. Antimicrob Agents Chemother 58:1302–1314. https://doi.org/10.1128/AAC.02098-13.

57. Pato ML. 1977. Tetracycline inhibits propagation of deoxyribonucleic acid replication and alters membrane properties. Antimicrob Agents Chemother 11:318–323. https://doi.org/10.1128/aac.11.2.318.

58. Huang H, Chen W, Pan J, Chen Q, Feng S, Yu Y, Chen Y, Su Y, Chen R. 2011. SERS spectra of a single nasopharyngeal carcinoma cell based on intracellularly grown and passive uptake Au nanoparticles. Spectroscopy 26:187–194. https://doi.org/10.1155/2011/971256.

59. Wei B, Cha SY, Yoon RH, Kang M, Roh JH, Seo HS, Lee JA, Jang HK. 2016. Prevalence and antimicrobial resistance of Campylobacter spp. isolated from retail chicken and duck meat in South Korea. Food Control 62:63–68. https://doi.org/10.1016/j.foodcont.2015.10.013.

60. Clinical and Laboratory Standards Institute (CLSI). 2018. Performance standards for antimicrobial disk and dilution susceptibility tests for bacteria isolated from animals, 5th ed. CLSI, Wayne, PA.

61. Feng J, Ma L, Nie J, Konkel ME, Lu X. 2017. Environmental stress-induced bacterial lysis and extracellular DNA release contribute to Campylobacter jejuni biofilm formation. Appl Environ Microbiol 84:e02068-17. https://doi.org/10.1128/AEM.02068-17.

62. Butler HJ, Ashton L, Bird B, Cinque G, Curtis K, Dorney J, Esmonde-White K, Fullwood NJ, Gardner B, Martin-Hirsch PL, Walsh MJ, McAinsh MR, Stone N, Martin FL. 2016. Using Raman spectroscopy to characterize biological materials. Nat Protoc 11:664–687. https://doi.org/10.1038/nprot.2016.036.

63. Wang S, Zhao J, Lui H, He Q, Zeng H. 2010. A modular Raman microspectroscopy system for biological tissue analysis. Spectroscopy 24:577–583. https://doi.org/10.1155/2010/592315.

64. Zhao J, Lui H, McLean DI, Zeng H. 2007. Automated autofluorescence background subtraction algorithm for biomedical Raman spectroscopy. Appl Spectrosc 61:1225–1232. https://doi.org/10.1366/000370207782597003.

65. Gautam R, Vanga S, Ariese F, Umapathy S. 2015. Review of multidimensional data processing approaches for Raman and infrared spectroscopy. EPJ Tech Instrum 2:1–38. https://doi.org/10.1140/epjti/s40485-015-0018-6.